Dual-Targeting Organometallic Ruthenium(II) Anticancer Complexes Bearing EGFR-Inhibiting 4-Anilinoquinazoline Ligands

ARTICLE *in* DALTON TRANSACTIONS · JUNE 2015

Impact Factor: 4.2 · DOI: 10.1039/C5DT01430A

7 AUTHORS, INCLUDING:

Wei Zheng
Chinese Academy of Sciences
15 PUBLICATIONS **104** CITATIONS
SEE PROFILE

Qun Luo
Chinese Academy of Sciences
29 PUBLICATIONS **201** CITATIONS
SEE PROFILE

Yao Zhao
Chinese Academy of Sciences
25 PUBLICATIONS **367** CITATIONS
SEE PROFILE

Fuyi Wang
Chinese Academy of Sciences
67 PUBLICATIONS **1,304** CITATIONS
SEE PROFILE

Dalton Transactions

PAPER

View Article Online
View Journal | View Issue

Cite this: *Dalton Trans.*, 2015, **44**, 13100

Dual-targeting organometallic ruthenium(II) anticancer complexes bearing EGFR-inhibiting 4-anilinoquinazoline ligands†

Yang Zhang,[a,b] Wei Zheng,*[a,b] Qun Luo,[a,b] Yao Zhao,[a,b] Erlong Zhang,[a,b,c] Suyan Liu[a,b] and Fuyi Wang*[a,b]

Received 15th April 2015,
Accepted 8th June 2015

DOI: 10.1039/c5dt01430a

www.rsc.org/dalton

We have recently demonstrated that complexation with (η^6-arene)Ru^{II} fragments confers 4-anilinoquinazoline pharmacophores a higher potential for inducing cellular apoptosis while preserving the highly inhibitory activity of 4-anilinoquinazolines against EGFR and the reactivity of the ruthenium centre to 9-ethylguanine (*Chem. Commun.*, 2013, **49**, 10224–10226). Reported herein are the synthesis, characterisation and evaluation of the biological activity of a new series of ruthenium(II) complexes of the type [(η^6-arene)Ru(*N*,*N*-L)Cl]PF_6 (arene = *p*-cymene, benzene, 2-phenylethanol or indane, L = 4-anilinoquinazolines). These organometallic ruthenium complexes undergo fast hydrolysis in aqueous solution. Intriguingly, the ligation of (arene)Ru^{II} fragments with 4-anilinoquinazolines not only makes the target complexes excellent EGFR inhibitors, but also confers the complexes high affinity to bind to DNA minor grooves while maintaining their reactivity towards DNA bases, characterising them with dual-targeting properties. Molecular modelling studies reveal that the hydrolysis of these complexes is a favourable process which increases the affinity of the target complexes to bind to EGFR and DNA. *In vitro* biological activity assays show that most of this group of ruthenium complexes are selectively active inhibiting the EGF-stimulated growth of the HeLa cervical cancer cell line, and the most active complex [(η^6-arene)Ru(*N*,*N*-L13)Cl]PF_6 (**4**, IC_{50} = 1.36 μM, **L13** = 4-(3′-chloro-4′-fluoroanilino)-6-(2-(2-aminoethyl)aminoethoxy)-7-methoxyquinazoline) is 29-fold more active than its analogue, [(η^6-arene)Ru(*N*,*N*-ethylenediamine)Cl]PF_6, and 21-fold more active than gefitinib, a well-known EGFR inhibitor in use clinically. These results highlight the strong promise to develop highly active ruthenium anticancer complexes by ligation of cytotoxic ruthenium pharmacophores with bioactive organic molecules.

Introduction

Ruthenium complexes have been regarded as the most promising metal based anticancer candidates due to many merits such as high selectivity, low toxicity and good water solubility during the past decades.[1–11] Ruthenium(III) complexes containing imidazole and/or indazole ligands have been deeply studied. Among them two complexes, namely NAMI-A and KP1019, exhibit *in vivo* activity against pulmonary metastases in all the solid tumors and certain types of tumours which are not successfully treatable with cisplatin,[12,13] respectively, and have already finished phase I clinical trials.[14–16] Meanwhile, half-sandwich arene ruthenium(II) complexes, which exhibit distinctive characteristics such as versatile structures and diverse modes of interaction with biomolecular targets, provide new possibilities for the development of metal based anticancer drugs. This type of ruthenium complexes present a "piano stool" geometry in which an η^6 π-bonded arene ligand forms the seat, and the three other ligands form the legs.[17–19] The hydrophobic arene ligands coordinate to ruthenium *via* a triple π–d bond, facilitating the passage of complexes through cell membranes, and the rest of the coordination sites around the Ru centre provide the opportunity to arrange diverse ligands to produce novel anticancer agents with distinct mechanisms of action.[1,4,6,7,20–25] Two classes of arene ruthenium(II) complexes of the types [(η^6-arene)Ru(en)Cl][PF_6] (en = ethylenediamine)[1,11,18,23,26–28] and (η^6-arene)Ru(pta)Cl_2 (pta =

[a]*Beijing National Laboratory for Molecular Sciences, Beijing 100190, PR China. E-mail: fuyi.wang@iccas.ac.cn, zhengwei0246@iccas.ac.cn; Fax: (+86)10-62529069; Tel: (+86)10-62529069*
[b]*CAS Key Laboratory of Analytical Chemistry for Living Biosystems, Institute of Chemistry, Chinese Academy of Sciences, Beijing 100190, PR China*
[c]*College of Chemistry and Materials Science, Key Laboratory of Functional Molecular Solids, The Ministry of Education, Anhui Laboratory of Molecular-Based Materials, Anhui Normal University, Wuhu 241000, P. R. China*
† Electronic supplementary information (ESI) available: Details for the synthesis of 4-anilinoquinazoline derivatives; data of NMR, HPLC, ELISA and MTT screening, and molecular modelling: Fig. S1–S19. See DOI: 10.1039/c5dt01430a

1,3,5-triaza-7-phosphatricyclo [3.3.1.1]-decane))[7–9,29–31] have demonstrated interesting *in vitro* and *in vivo* anticancer activity. Studies of the structure activity relationship suggested that the arene ligands, the ruthenium(II) centre and the mono-/chelating ligands play distinct yet synergetic roles in tuning the biological activities of these complexes.[7,11,18]

Recently, we have designed and synthesised a series of ruthenium(II) complexes by modifying the prototype [(η^6-arene)-Ru(en)Cl][PF_6] (en = ethylenediamine) complexes at the en chelating ligand with 4-anilinoquinazolines,[32,33] which are analogues of the well-established epidermal growth factor receptor (EGFR) inhibitor gefitinib currently used for clinical treatment of locally advanced or metastatic non-small cell lung cancer (NSCLC).[34,35] The introduction of the anilinoquinazoline pharmacophores confers the resulting ruthenium complexes high inhibitory potential for EGFR while preserving the reactivity of the Ru centre towards the DNA model compound 9-EtG.[33] In turn, complexation with the cytotoxic organometallic ruthenium fragments enhances the ability of the anilinoquinazolines to induce apoptosis, in particular early-stage apoptosis. Intriguingly, some of the bifunctional ruthenium arene complexes exhibited higher anticancer activity than the cytotoxic complex [(η^6-*p*-cymene)Ru(en)Cl]PF_6[1] and gefitinib[34,35] towards the MCF-7 human breast cancer cell line, implying a promising type of dual-targeting anticancer agents.[32]

As a continuous effort, in the present work, we have synthesised and characterised a series of novel organometallic ruthenium(II) complexes bearing different arene ligands and diverse 4-anilinoquinazoline derivatives as chelating ligands. The inhibitory potency against EGFR and reactivity towards calf thymus DNA (ctDNA) of the newly synthesised complexes were investigated, followed by evaluation of their antiproliferative activity towards the HeLa human cervical cancer cell line. Moreover, molecular modelling was performed to study and visualise the interactions of this group of organometallic ruthenium complexes with EGFR and DNA to further establish their structure and activity relationship.

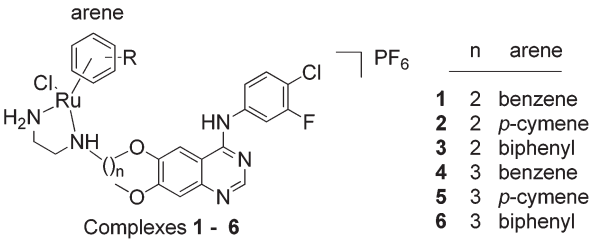

Fig. 1 Chemical structures of complexes **1–6**.

Results and discussion

Synthesis and characterisation

To introduce suitable bioactive groups to the cytotoxic ruthenium(II) arene complexes of the type [(η^6-arene)Ru(en)Cl][PF_6], we have recently synthesised a couple of en derivatives using EGFR inhibiting 4-anilinoquinazolines to modify one of the NH_2 groups.[32] The reactions of the resulting en derivatives with ruthenium arene dimers [(η^6-arene)$RuCl_2$]$_2$ (arene = benzene, *p*-cymene and biphenyl) gave rise to six organometallic ruthenium(II) complexes **1–6** shown in Fig. 1.[32] In this work, we employed 2-phenylethanol, indane, *p*-cymene and benzene as arene groups attached to the ruthenium centre, and 3-chloro-4-fluoro-anilino, 3-cyanoanilino, 3-methoxy-anilino as substituents at the 4-position of the quinazoline ring to prepare new organometallic ruthenium(II) complexes bearing EGFR-inhibiting anilinoquinazoline ligands. The 4-anilinoquinazoline derivatives were synthesised following a modified method described in our previous work.[32] 7-methoxy-4-oxo-3,4-dihydroquinazolin-6-yl-acetate was used as the starting material,[36] anilinoquinazoline derivatives **L13–L16** were synthesised with moderate yields (Scheme 1). Then these 4-anilinoquinazolines reacted with the designated arene ruthenium(II) dimer [(arene)$RuCl_2$]$_2$ (arene = *p*-cymene, benzene, 2-phenylethanol or indane) to produce the target complexes **7–14**, respectively.

The as-prepared complexes were characterised using ^{1}H and ^{13}C NMR (Fig. S1–S8 in the ESI†), elemental analysis and MS, and the details are given in the Experimental section. Similar to complexes **1–6**, due to the modification of the en chelating ligands, each of the complexes **7–14** contains two stereogenic centres, giving rise to four possible configurations. Sadler and co-workers have reported that the chemical shifts of the proton at the –NHR group in the en ligands of four configurations may be different from each another, which can be used to identify the configurations of this type of chiral

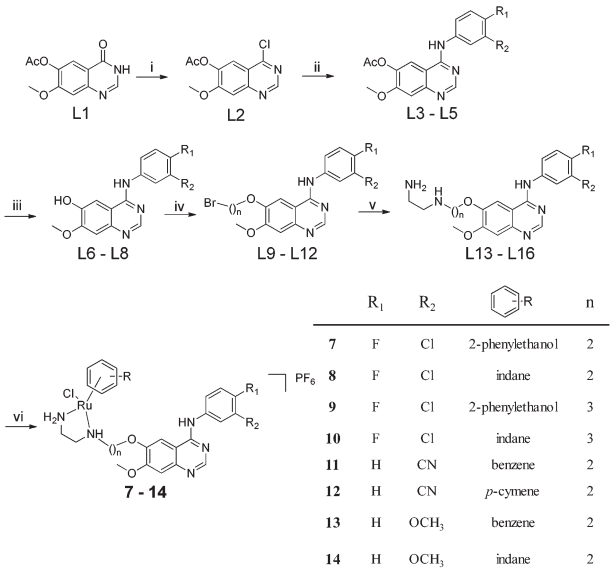

	R_1	R_2	R	n
7	F	Cl	2-phenylethanol	2
8	F	Cl	indane	2
9	F	Cl	2-phenylethanol	3
10	F	Cl	indane	3
11	H	CN	benzene	2
12	H	CN	*p*-cymene	2
13	H	OCH_3	benzene	2
14	H	OCH_3	indane	2

Scheme 1 Synthesis of complexes **7–14**. Reaction conditions: (i) $SOCl_2$, DMF; (ii) substituted aniline, isopropanol; (iii) CH_3ONa, CH_3OH; (iv) 1,2-dibromoethane or 1,3-dibromopropane, K_2CO_3, DMF; (v) ethylenediamine, CH_3CN; (vi) [(η^6-arene)$RuCl_2$]$_2$, NH_4PF_6, CH_3OH. Details and yields are given in the Experimental section and the ESI.†

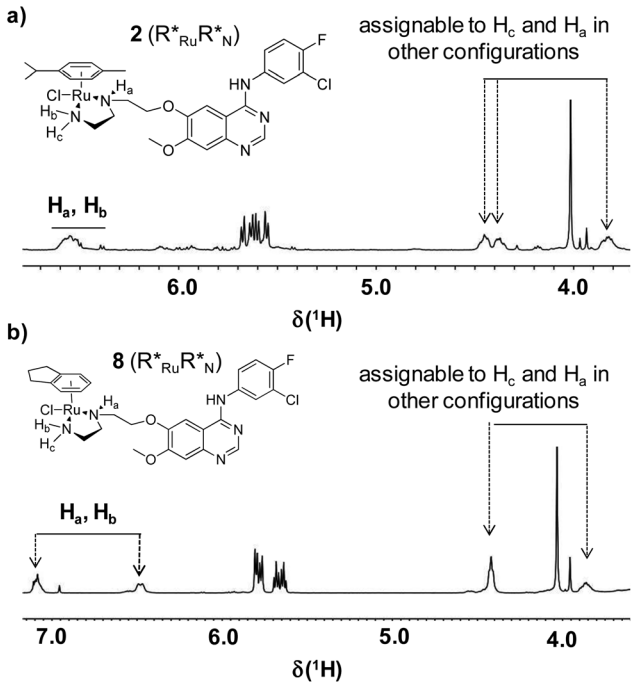

Fig. 2 ^{1}H NMR spectra of (a) complex **2** and (b) complex **8** in d_6-DMSO over the range of 7.2 to 3.6 ppm.

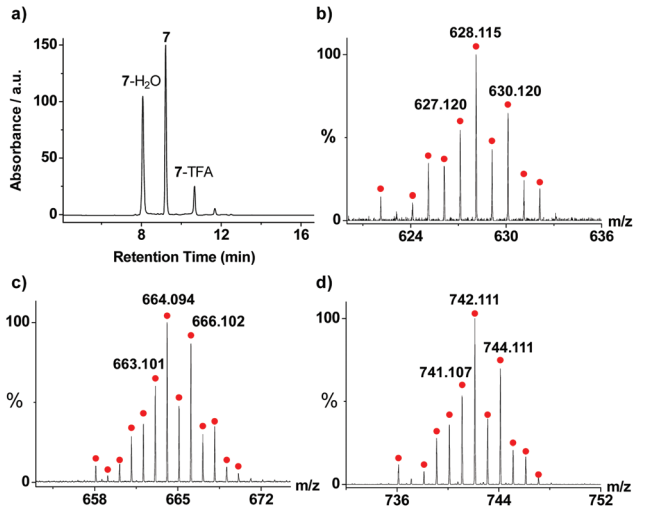

Fig. 3 (a) HPLC chromatogram with UV detection at 360 nm of complex **7** (0.1 mM) in aqueous solution incubated at 298 K for 2 h. (b–d) Mass spectra for HPLC fractions shown in (a): (b) **7**-H_2O ({[**7**-H_2O] – H_2O – PF_6}$^+$, *m/z* theoretical: 628.106, experimental: 628.115); (c) **7** ({**7** – PF_6}$^+$, *m/z* theoretical: 664.083, experimental: 664.094); (d) **7**-TFA ({[**7**-TFA] – PF_6}$^+$, theoretical: 742.099, experimental: 742.111). The red spots represent the simulated isotopic patterns of the respective species.

complex.[37] As shown in Fig. 2, the ^{1}H NMR results obtained for the d_6-DMSO solutions of complexes **2** and **8** indicate that there is indeed more than one stereoisomer co-existing in the solutions. We have previously produced monoclinic crystals of complex **2** by the slow diffusion of diethyl ether into its methanol solution, which was identified by X-ray diffraction analysis as the $R^*_{Ru}R^*_N$ configuration.[32] However, attempts to gain crystals of the other complexes were not successful. Thus, all the chiral ruthenium complexes in this work were used as a mixture of four stereoisomers.

Hydrolysis

The hydrolysis of arene ruthenium(II) complexes containing chloride ligands is thought to be the essential step to activate them towards biomolecules.[11,28,37–39] In our previous work, we also demonstrated that complexes **1–6** underwent hydrolysis in aqueous solution at similar rates to those of the respective en complexes [(η^6-arene)Ru(en)Cl]$^+$ (arene = benzene, *p*-cymene or biphenyl).[33,40] Herein, the hydrolysis of the newly synthesised complexes **7–14** was studied by HPLC-MS and UV-Vis spectroscopy. The chromatograms of HPLC, which were obtained by analysis of the aqueous solution of each complex (0.1 mM) incubated in water for 2 h under ambient temperature, are shown in Fig. 3a and S9 in the ESI.† In general, three fractions were observed in the chromatogram of each complex. For example, as shown in Fig. 3a, there are three species eluting at 8.06, 9.21 and 10.67 min from the analysis of the aqueous solution of complex **7**, which were identified by ESI-MS (Fig. 3b–d) to be the hydrolytic adduct (**7**-H_2O), intact **7** and the TFA adduct (**7**-TFA), respectively. The TFA adduct was formed by the substitution of an aqua ligand in the hydrolytic adduct by TFA which was used as an ion-pairing agent in HPLC separation.[40] Furthermore, we determined the hydrolytic rates of compounds **7–14** using UV-Vis spectroscopy (Fig. S10†). The isosbestic points in the differential UV-Vis spectra indicated that the hydrolysis of Ru–Cl is a kind of first order reaction. The time-dependent changes (A) in absorbance at a selected wavelength for each complex (Fig. S11†) were fitted to the first order reaction rate equation, giving rate constants (k) and half-lives ($t_{1/2}$) of complexes **7–14** as shown in Table 1. The results indicate that all the half-lives of hydrolysis of these complexes are less than 60 min, suggesting that the hydrolysis of complexes **7–14** can reach equilibrium within 2 h. The equilibrium constants (K) were calculated on the basis of the HPLC peak areas (Fig. S9†) to be 1.11, 0.98, 1.36, 4.22, 0.83, 0.87, 1.21, and 1.22 for **7–14**, respectively. These indicate that complexes **9** and **10**, which consist of C3-alkyl linkers, were more sensitive to hydrolysis than the other complexes containing C2-alkyl linkers.

Interactions with calf thymus DNA

Ruthenium complexes are well documented to bind to DNA covalently and non-covalently. It has been demonstrated that arene ruthenium(II) complexes of the type of (arene)Ru^{II}(en) preferentially bind at N7 of the guanine base *via* Ru–N coordination, accompanied by the intercalation of the non-coordinated aromatic rings in the arene ligands between adjacent bases.[17,38,41,42] Here we selected complexes **4** and **8** to investigate the interactions of this series of organometallic ruthenium complexes containing a 4-anilinoquinazoline

Table 1 The hydrolysis rate constants (k), half-lives ($t_{1/2}$), IC_{50} for the inhibition of EGFR activity and of the growth of the HeLa cancer cell line of complexes **1–14**

Compound	k ($\times 10^{-4}$ s^{-1})/ $t_{1/2}$ (min)	IC_{50} for EGFR[a] (nM)	IC_{50} for HeLa[b] (μM)	
			−EGF	+EGF
RM116	—[c]	—	25.4 ± 4.4	40.1 ± 2.6
Cisplatin	—	—	14.6 ± 3.2	—
Gefitinib	—	94.0 ± 3.1	41.5 ± 3.8	29.5 ± 2.6
1	3.60/32.1[d]	20.3 ± 3.3[d]	50.8 ± 3.3	31.1 ± 2.4
2	3.58/32.2[d]	63.1 ± 1.5[d]	45.2 ± 4.1	42.8 ± 2.4
3	3.48/33.2[d]	118.6 ± 7.9[d]	38.8 ± 2.7	40.0 ± 4.5
4	4.81/24.0[d]	29.1 ± 3.4[d]	4.60 ± 1.6	1.36 ± 0.34
5	5.00/23.1[d]	33.2 ± 7.3[d]	61.7 ± 8.7	37.1 ± 2.6
6	10.6/10.8[d]	81.7 ± 7.2[d]	38.6 ± 6.2	25.4 ± 5.1
7	5.12/22.5	62.5 ± 7.3	64.4 ± 12.2	33.3 ± 11.3
8	3.81/30.3	70.7 ± 14.1	34.8 ± 4.4	19.0 ± 5.2
9	3.45/33.5	34.4 ± 1.0	59.0 ± 4.1	16.6 ± 4.5
10	1.95/59.2	22.3 ± 6.7	45.2 ± 4.0	21.7 ± 1.5
11	2.88/40.2	139.4 ± 17.5	59.5 ± 6.4	90.6 ± 9.1
12	3.15/36.7	167.2 ± 13.5	101.4 ± 11.3	67.3 ± 8.2
13	3.26/35.4	64.0 ± 8.3	63.5 ± 6.6	69.5 ± 8.7
14	4.86/23.7	167.4 ± 3.1	63.1 ± 12.0	75.8 ± 3.0

[a] IC_{50} values were determined in the presence of 200 μM ATP (n = 3). [b] The HeLa cells were incubated with each compound for 48 h (n = 6). [c] Not applicable. [d] Data cited from our previous work (ref. 33).

ligand with calf thymus DNA (ctDNA) by using circular dichroism (CD) spectroscopy. As shown in Fig. 4, the interactions of ctDNA with complexes **4** and **8** not only reduced the positive band centred at 275 nm with a slight blue-shift, but also induced a change in the profile of the CD spectrum of ctDNA, leading to the appearance of small negative bands centred at *ca.* 325 nm (for **4**) and 300 nm (for **8**), respectively. The characteristic CD spectrum of ctDNA in B-form usually consists of a positive band centred at 275–280 nm and a negative band at about 245 nm which are attributed to base stacking and helicity, respectively.[43] It has been reported that apart from coordinating with guanine bases, the ruthenium complexes containing multi-ring arene ligands such as biphenyl, dihydroanthracene, and tetrahydroanthracene can intercalate between the bases of ctDNA *via* π–π stacking, enhancing the intensity of the absorption band at 275 nm, while the ruthenium complexes bearing mono-hydrocarbon ring ligands, *e.g.* *p*-cymene, only bind to G–N7, reducing the intensity of this positive band probably due to disruption to the base stacking of DNA.[44] Palaniandavar and co-workers have shown that metal-bindings at the groove of ctDNA usually lead to shape transformation of the CD profile.[45] Collectively, our CD spectroscopic studies indicate that the interaction of ctDNA with complexes **4** and **8**, which contain a multi-ring 4-anilinoquinazoline ligand and a mono-ring arene ligand (benzene and indane, respectively), involve both base coordination and groove binding.

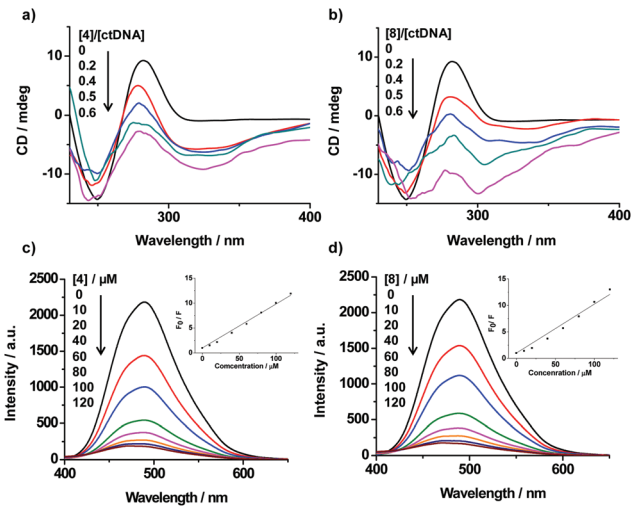

Fig. 4 (a and b) CD Spectra of ctDNA (200 μM in base pairs) treated with different concentrations of (a) complex **4** or (b) complex **8**. (c and d) Fluorescence titration of a ctDNA–Hoechst complex (ctDNA : Hoechst = 200 : 20 μM) by (c) complex **4** or (d) complex **8**. The insets are the Stern–Volmer plots for the quenching of the fluorescence intensity of the ctDNA–Hoechst complex by complex **4** or **8** (0–120 μM).

To verify the groove binding of complexes **4** and **8** to ctDNA, we performed competition assays using the DNA minor groove binder Hoechst33342. The fluorescent ctDNA–Hoechst complex illuminates at 400–650 nm with a maximum of 490 nm upon excitation at 370 nm (Fig. 4). With the addition of complex **4** or **8**, the emission of the ctDNA–Hoechst complex significantly decreased in intensity. The obtained Stern–Volmer plots for the quenching of the fluorescence intensity of ctDNA–Hoechst by complexes **4** and **8** give rise to K_{sv} constants of 8.8×10^4 M^{-1} and 9.2×10^4 M^{-1}, respectively, indicating that these ruthenium complexes are competitive minor groove binders to DNA.[46]

EGFR inhibition

Next, we performed an enzyme-linked immunosorbent assay (ELISA) to evaluate the EGFR inhibitory activities of complexes **7–14**. The well-established EGFR inhibitor gefitinib was used as the reference. The IC_{50} value of gefitinib to EGFR has been reported to be 33 nM in the presence of 5 μM of ATP.[34] In this study, the concentration of ATP was set at 200 μM and the IC_{50} of gefitinib was measured to be 94 nM. Under the same conditions, the dose-dependent curves of enzyme inhibition for complexes **7–14** are shown in Fig. S12,† and the IC_{50} values are listed in Table 1. Combined with the IC_{50} values of complexes **1–6** reported in our previous work,[33] we found the EGFR inhibitory activities of complexes **1**, **2**, **4–10** and **13** are better than gefitinib. We have previously authenticated that the complexation of arene ruthenium(II) complexes, where the arene ligand was *p*-cymene, benzene or biphenyl, to the 6-methoxy position of 4-anilinoquinazoline *via* an alkyl linker has little effect on the EGFR inhibitory capacity of the 4-anilinoquinazoline pharmacophore, and complexes containing C3 linkers are more active towards EGFR than the respective analogues containing C2 linkers. The present results indicate that the phenylethanol complex **9** containing a C3 linker is more active than its analogue **7** with a C2 linker to EGFR, while the indane complex **10** is a better EGFR inhibitor than its analogue **8**,

further evidencing this structure activity relationship. However, when 3-chloro-4-fluoroanilino was replaced by 3-cyanoanilino or 3-methoxy at the 4-position of quinazoline, the inhibitory potential against EGFR of the resulting complexes was reduced, indicating that the strong electronic withdrawing groups Cl and F at the aniline moiety are more favourable than the cyanide and methoxy substituents in terms of EGFR inhibition for this series of ruthenium complexes.

Antiproliferation potency

We next employed a MTT (3-(4,5-dimethyl-2-thiazolyl)-2,5-diphenyl-2-H-tetrazolium bromide) assay to evaluate the antiproliferative activities of complexes **1–14** towards the HeLa human cervical cancer cell line that has been reported to overexpress EGFR.[47] The clinically used anticancer drug gefitinib, cytotoxic anticancer agents RM116 ([(η^6-*p*-cymene)Ru(en)Cl]-PF_6)[1,19] and cisplatin were chosen as the positive controls. The dose-dependent antiproliferative curves either in the presence or in the absence of additional epidermal growth factor (EGF) are shown in Fig. S13 and S14,† and the resulting IC_{50} values are listed in Table 1.

As anticipated, the EGFR-inhibiting gefitinib exhibited apparent EGF-dependent antiproliferative activity towards the HeLa cell line with IC_{50} values of 29.5 μM in the presence of EGF and 41.5 μM in the absence of EGF, respectively, which has been thought to be attributed to its blocking of the downstream signalling pathway initiated by autophosphorylation of EGFR.[34] Interestingly, our antiproliferation assay results show that the arene ruthenium complexes **1**, **4–10**, and **12** also exhibit selective inhibitory activity on the EGF-stimulated growth of the HeLa cell line, among them complexes **4**, **6**, **8**, **9** and **10** are more active than gefitinib against EGF-induced growth of HeLa cells. Complex **4** was demonstrated to be the most active agent inhibiting the growth of the HeLa cell line, against which the activity is even higher than the cytotoxic metallodrug cisplatin. The MTT results also indicate that those complexes, which did not show EGF-dependent antiproliferative potency, usually accomplished relatively weak EGFR inhibitory activities. On the other hand, in the absence of exogenous EGF, most of the tested complexes also exhibited inhibitory activity against HeLa cells, suggesting that besides blocking the EGFR signalling, these complexes act as anticancer agents through other mechanisms, *e.g.* attacking DNA as they have been shown to be effective DNA binders *via* both base coordination and minor groove binding (*vide supra*).

The antiproliferative activity on non-tumorigenic human bronchial epithelial (HBE) cells was studied to evaluate the selectivity of these complexes. At a concentration of 50 μM, the inhibition values of complexes **7–14** against HBE cells were less than 50% (data not shown). The dose-dependent antiproliferative curves of complex **8** are depicted in Fig. S15.† The IC_{50} values of complex **8** were measured to be 54.7 μM and 75.6 μM in the presence and in the absence of EGF, respectively. The more than 2-fold higher cytostatic activity to cancer cells than to non-malignant cells verified the good selectivity of the ruthenium anticancer complexes in the antiproliferation of cancer cells.

Molecular modelling

In order to verify further the dual-targeting properties of the synthesised ruthenium complexes, we performed a molecular modelling study by docking the ruthenium complexes to the EGFR kinase domain and to DNA *via* either G–N7 coordination or minor groove binding using the Surflex-dock module built in the Sybyl-X 1.1 programme.[48,49] The docking scores generated by the docking analysis for binding to EGFR and the DNA minor groove are the weighted sum of the nonlinear functions of the exposed atomic van der Waals surface distances of the protein (or DNA)–ligands expressed in $-\lg K_d$ [50] that can be used to evaluate the affinity between the ligands and receptors. For the Ru–N7(–G) coordination, the molecular modelling generates the binding energy in kcal mol^{-1}, the larger the absolute value of the binding energy is, the stronger the Ru–N bond is.

There are two chiral centres (Ru* and N*) in each complex, which results in four stereoisomers.[37] Firstly, we determined the docking scores of the four stereoisomers of complex **8** into the ATP-binding pocket of EGFR and into the minor groove of a B-form DNA duplex 5′-d(CGCGAATTCGCG)·d(CGCGAATTCGCG)-3′ (**I**),[51] and no pronounced difference in the scores of the different stereoisomers was found, though the docking conformations were quite distinctive (Fig. S16†). In addition, no significant difference was found for the binding energy of the four stereoisomers of **8** to N7 of G4 in **I** (Fig. S17†). Therefore, only the docking scores to EGFR and DNA **I**, and the binding energy to G4–N7 in **I** of the $R^*_{Ru}R^*_N$ configuration of each complex are listed in Table 2. The G4 base was chosen as the coordination site as (arene)Ru complexes were shown to bind preferentially to the guanine bases in the

Table 2 Docking scores into the EGFR kinase domain and into the DNA minor groove as well as binding energy (kcal mol^{-1}) to G–N7 in the DNA duplex **I** of complexes **1–14** and their aqua adducts

	Docking score			Docking score		
Cmpd	To EGFR	To DNA	Cmpd	To EGFR	To DNA	Binding energy to G–N7
RM116	—[a]	—	RM116-H_2O	—	—	−104
Cisplatin	—	—				
Gefitinib	6.80	4.05	$Pt(NH_3)_2$-$Cl(H_2O)$	—	—	−128
1	9.40	5.46	**1**-H_2O	10.21	6.92	−123
2	8.76	4.61	**2**-H_2O	9.07	6.91	−112
3	8.51	6.03	**3**-H_2O	8.21	7.24	−130
4	10.04	5.68	**4**-H_2O	10.14	7.13	−125
5	8.88	5.26	**5**-H_2O	10.06	6.57	−106
6	8.93	5.39	**6**-H_2O	9.02	7.41	−133
7	7.44	4.32	**7**-H_2O	9.43	6.04	−107
8	6.94	5.27	**8**-H_2O	9.07	6.71	−119
9	9.65	6.25	**9**-H_2O	10.19	6.74	−103
10	7.56	4.67	**10**-H_2O	10.15	7.44	−98
11	6.85	4.09	**11**-H_2O	8.59	6.70	−125
12	6.31	5.53	**12**-H_2O	8.57	6.04	−95
13	7.27	6.70	**13**-H_2O	9.92	7.36	−105
14	6.25	4.17	**14**-H_2O	8.41	5.95	−96

[a] Not applicable.

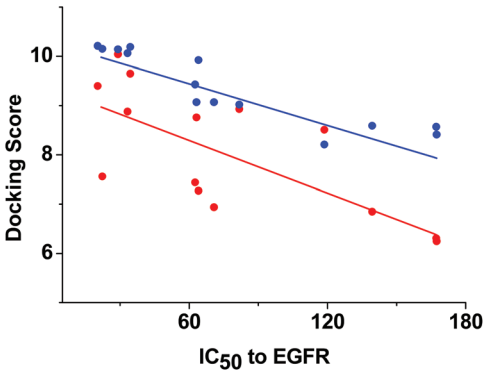

Fig. 5 Plots of the docking scores of complexes **1–14** (red) as well as their hydrolytic adducts (blue) to EGFR *vs.* IC_{50} to EGFR (nM). The regression (*R*) values for both linear fits were calculated to be 0.683 (red) and 0.896 (blue).

middle region of DNA duplexes.[52] On the other hand, since this group of ruthenium complexes could be hydrolysed in aqueous solution, the molecular modelling was also performed on the hydrolytic species of all the ruthenium complexes.

As shown in Fig. 5 and Table 2, the docking scores of ruthenium complexes **1–14** and their hydrolytic adducts to the ATP-binding pocket of EGFR are in good agreement with their IC_{50} inhibiting EGFR activities (Table 1), *i.e.* the higher the docking scores are, the higher the inhibitory potency values of the corresponding complexes against EGFR are. Taking complex **8** as an example, the typical conformations of the ruthenium arene complexes and their hydrolytic adducts binding to the ATP-binding pocket of EGFR are shown in Fig. 6a and b. It can be seen that complex **8** and its hydrolytic adduct employed similar binding poses to that of erlotinib at the ATP-binding cleft of EGFR[53] in that the 4-position substituted aniline

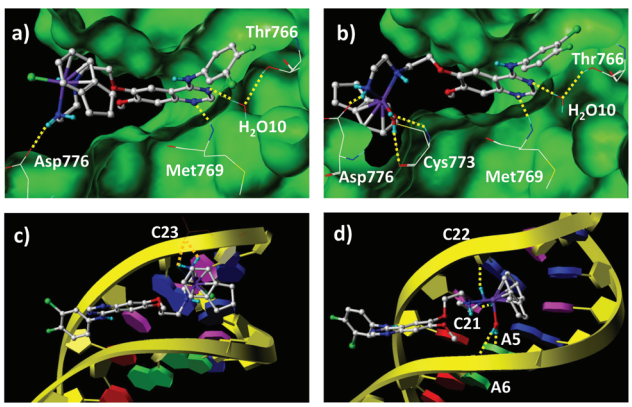

Fig. 6 (a and b) The detailed conformation of the ATP-binding pocket housing the cation of (a) complex **8** or (b) **8** in aqua form; (c and d) docking poses of the cation of (c) complex **8** or (d) **8** in aqua form into the minor groove of DNA duplex **I**. The residues of EGFR are shown in stick form with O atoms in red, N atoms in blue, S atoms in yellow and C atoms in grey; duplex **I** is shown in ribbon form with G in blue, C in pink, A in green and T in red. The dotted yellow lines illustrate the positions of the H-bonding interactions.

entered into the hydrophobic cavity of EGFR *via* a low energy conformation: the N3 of the quinazoline group was H-bonded to Thr766 through a water bridge, and the N1 accepted an H-bond to the N–H group of Met769. These H-bonds were thought to be crucial to stabilise the conformation of the EGFR-inhibitor complexes. These results suggest that the complexation of 4-anilinoquinazolines with the bulky arene ruthenium(II) fragments has little disruption to the interaction of the EGFR-inhibiting pharmacophores with EGFR. It is notable that the replacement of Cl by H_2O in **8** leads to the formation of additional H-bonds between the hydrolytic adduct and Cys773 in EGFR (Fig. 6b). In some cases, the hydrolytic species could form additional H-bonds either with Asp776 or Leu694 that are located at the edge of the ATP-binding cleft. For instance, the hydrolytic adduct of complex **2** forms an H-bond between its aqua ligand and Asp776 (Fig. S18†), and the aqua ligand in hydrolytic **4** forms H-bonds with both Asp776 and Leu694 (Fig. S19†). The formation of additional H-bonds due to hydrolysis of the ruthenium complexes appears to increase the affinity of the inhibitors for EGFR so that the docking scores of most of the hydrolytic species are slightly higher than those of the respective chloride complexes (Fig. 5), implying that the hydrolytic adducts of the tested ruthenium complexes may contribute more to the EGFR inhibitory potential than the respective chloride species. This leads to a better linearity (R = 0.896) between the IC_{50} values and the docking scores to EGFR of the mono-aquated ruthenium complexes than that (R = 0.6834) between the IC_{50} values and the docking scores to EGFR of the parent ruthenium chloride complexes (Fig. 5). In other words, the hydrolytic adducts of the ruthenium complexes are more active than the respective chloride complexes against EGFR.

The minor groove of DNA is thought to be an essential binding site for small molecules.[54] Our CD spectroscopy and fluorescent titration results have shown that the ligation of the (arene)Ru(en) units with 4-anilinoquinazoline derivatives allow the resulting complexes to bind to the minor groove of ctDNA (Fig. 4) apart from the well-established G–N7 coordination.[17,38,41] Therefore, complexes **1–14** and their hydrolytic species were mounted into the minor groove of the B-form dodecamer duplex **I**[51] for docking analysis, and the scores are listed in Table 2. The high docking scores, ranging from 4.09 to 7.44, indicate that the introduction of the 4-anilinoquinazoline ligands indeed confers the arene ruthenium complexes with high affinity binding to the DNA minor grooves. Similar to EGFR binding, the scores of the hydrolytic species binding to the DNA minor grooves were significantly higher than those of their parent chloride complexes, indicating that hydrolysis is also favourable for the DNA minor groove binding. As shown in Fig. 6c and d, the hydrolysis of complex **8** induces the formation of two more H-bonds between the complex and bases, contributing to the higher affinity of the hydrolytic adducts to the minor groove compared with the chloride species.

It has been well established that arene ruthenium(II) complexes are inclined to bind covalently to G–N7 of DNA after hydrolysis.[17,38,55] In the present work, the covalent binding of

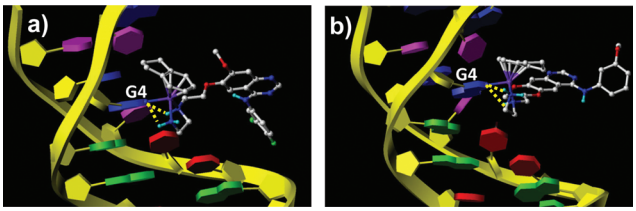

Fig. 7 The detailed conformations of the cations of (a) complex **8** and (b) complex **14** covalently bound to the N7 of G4 in DNA duplex **I**. The duplex **I** is shown in ribbon form with G in blue, C in pink, A in green and T in red. The dotted yellow lines illustrate the positions of the H-bonding interactions.

complexes **1–14** to G–N7 in DNA duplex **I** were also evaluated by means of calculating the binding energy. The results are listed in Table 2 and the details of the typical binding conformations are shown in Fig. 7. The results indicate that these complexes possess a high potential to bind to DNA covalently (binding energy ranged from −133 to −95 kcal mol^{-1}), that was comparable to that of cisplatin (−128 kcal mol^{-1}). Fig. 7 demonstrates that both complexes **8** and **14** locate in the major groove of duplex **I** with a coordination bond between Ru–N7(–G4) and two H-bonds form between G4 and the modified en group. These H-bonds could help to stabilise the conformation, conferring the high selectivity of this type of ruthenium complex to guanine bases.[17]

Conclusions

In this work, a series of arene ruthenium(II) complexes containing 4-anilinoquinazoline ligands were synthesised and characterised, their inhibitory activities against EGFR and reactivity towards DNA were investigated and their activities inhibiting the growth of the HeLa cancer cell line were subsequently evaluated. The results indicate that ligation of organometallic ruthenium fragments with EGFR-inhibiting 4-anilinoquinazolines confers the resulting complexes with dual-targeting properties, *i.e.* a high potential for inhibiting EGFR activity and high reactivity towards DNA. Intriguingly, most of the newly synthesised ruthenium complexes exhibit selectively antiproliferative potency on the EGF-stimulated growth of the HeLa cancer cell line. Molecular modelling reveals that the hydrolysis of the organometallic ruthenium complexes increases their inhibitory activity against EGFR and reactivity towards DNA, promoting their anticancer potential. These findings provide novel insights into the rational design of novel ruthenium based anticancer complexes with multi-targeting functions.

Experimental

Materials

The 7-methoxy-4-oxo-3,4-dihydroquinazolin-6-yl-acetate (AR grade) was purchased from Shanghai FWD Chemicals Co. (China); 1,2-dibromoethane, and 1,3-dibromopropane from Beijing Ouhe Technology Co. (China); $[(\eta^6\text{-}p\text{-cymene})RuCl_2]_2$ from Beijing InnoChem Science & Technology Co. (China); $[(\eta^6\text{-benzene})RuCl_2]_2$, $[(\eta^6\text{-phenylethanol})\text{-}RuCl_2]_2$, and $[(\eta^6\text{-indane})RuCl_2]_2$ were kindly provided by Professor Peter Sadler and Dr Abraha Habtemariam. Thin layer chromatography silica gel was purchased from the Yantai Institute of Chemical Industry Research (China), and the silica gel column from Qingdao Jiyida Silica Reagent Manufacture (China); organic solvents including absolute methanol, absolute ethanol, acetone, acetonitrile, dichloromethane, diethyl ether and DMF were analytical grade and used directly without further purification. The deionized water was prepared by a Milli-Q system (Millipore, Milford, MA).

Synthesis and characterisation of 4-anilinoquinazoline derivatives

Compounds **L2–L8** were synthesised following the methods reported in the literature with slight modification, and **L9–L14** were synthesised according to the procedures described in our previous work.[32] The details for the syntheses are given in the ESI.†

Synthesis of compound L15. 4-(3-Cyanoanilino)-6-(2-bromoethoxy)-7-methoxyquinazoline (0.5 g, 1.14 mmol) was dissolved in 20 mL acetonitrile and then ethylenediamine (0.8 mL, 12 mmol) was added. The resulting mixture was heated to reflux and stirred for 2.5 h. Then the solvent was evaporated under vacuum and the residue was chromatographed by flash chromatography on silica gel using methanol/dichloromethane/ammonia (1 : 20 : 0.1) as the eluent to give compound **L15** as a white powder (0.36 g, 75.3%).^{1}H NMR (d_6-DMSO, 400 MHz) δ (ppm): 8.54 (s, 1 H), 8.37 (s, 1 H), 8.15 (d, J = 8.0 Hz), 7.88 (s, 1 H), 7.58 (t, J = 8.0 Hz, 1 H), 7.23 (s, 1 H), 4.21–4.19 (m, 2 H), 3.95 (s, 3 H), 3.00 (t, J = 5.6 Hz, 2 H), 2.70–2.60 (m, 4 H). ESI-MS (m/z): 379.1 ($[M + H]^+$, $C_{20}H_{23}N_6O_2$ requires 379.2).

Synthesis of compound L16. 4-(3-Methoxyanilino)-6-(2-bromoethoxy)-7-methoxyquinazoline (0.5 g, 1.14 mmol) was dissolved in 20 mL acetonitrile and then ethylenediamine (0.8 mL, 12 mmol) was added. The resulting mixture was heated to reflux and stirred for 2.5 h. Then the solvent was evaporated under vacuum and the residue was chromatographed by flash chromatography on silica gel using methanol/dichloromethane/ammonia (1 : 20 : 0.1) as the eluent to give **L16** as a white powder (0.38 g, 80.2%). ^{1}H NMR (d_6-DMSO, 400 MHz) δ (ppm): 8.74 (s, 1 H), 8.06 (s, 1 H), 7.41–7.35 (m, 2 H), 7.30–7.24 (m, 2 H), 6.87 (d, J = 8.0 Hz, 1 H), 6.55 (br s, 1 H), 4.47 (br s, 1 H), 4.40 (br s, 2 H), 4.04 (s, 3 H), 3.96–3.89 (m, 2 H), 3.81 (s, 3 H), 3.67–3.58 (m, 2 H), 2.91–2.78 (m, 2 H), 2.74–2.67 (m, 2 H). ESI-MS (m/z): 384.1 ($[M + H]^+$, $C_{20}H_{26}N_5O_3$ requires 384.2).

General procedure for the preparation of arene ruthenium(II) complexes 7–14

The as-prepared compounds **L13–L16** (0.26 mmol) and corresponding ruthenium(II) dimer $[(\eta^6\text{-arene})RuCl_2]_2$ (0.13 mmol)

were dissolved in methanol (10 mL), and the mixture was heated to reflux and stirred for 4 h and filtered. Then ammonium hexafluorophosphate (0.39 mmol) was added to the solution and further stirred for 10 min. The solvent was removed under vacuum and the residue was chromatographed by flash chromatography on silica gel using methanol/dichloromethane/ammonia (1 : 20 : 0.2) as the eluent to give the target products.

Complex 7. Yellow powder (65.6 mg, 31.2%). Anal. Calc. for $C_{27}H_{31}Cl_2F_7N_5O_3PRu{\cdot}2H_2O$: C, 38.35; H, 4.17; N, 8.28%. Found: C, 38.30; H, 4.26; N, 8.21. ^{1}H NMR (d_6-DMSO, 400 MHz) δ (ppm): 8.87 (s, 1 H), 8.10 (s, 1 H), 8.02 (dd, J_1 = 6.8 Hz, J_2 = 2.4 Hz, 1 H), 7.70–7.67 (m, 1 H), 7.58 (t, J = 2.8 Hz, 1 H), 7.32 (s, 1 H), 7.26–7.20 (m, 1 H), 6.68 (br s, 1 H), 5.83 (t, J = 5.6 Hz, 1 H), 5.61 (t, J = 5.6 Hz, 1 H), 5.57 (d, J = 6.0 Hz), 4.45 (s, 2 H), 4.07 (s, 3 H), 3.88–3.86 (m, 1 H), 3.69 (t, J = 6.0 Hz, 2 H), 3.58–3.54 (m, 1 H), 2.69–2.65 (m, 2 H), 2.63–2.59 (m, 2 H), 2.34–2.31 (m, 1 H), 2.07–1.98 (m, 1 H). ^{13}C NMR (d_6-DMSO, 100 MHz) δ (ppm): 158.5, 156.8, 150.4, 149.3, 134.8, 126.9, 125.6, 120.0, 119.8, 117.7, 117.5, 107.8, 104.6, 101.5, 84.7, 84.3, 83.4, 81.5, 80.4, 79.8, 68.3, 60.5, 57.2, 53.7, 51.8, 45.9, 36.3. MS (MALDI-TOF) (m/z): 664.2 (M^+, $C_{27}H_{31}Cl_2FN_5O_3Ru$ requires 664.1); 628.2 ($[M - HCl]^+$, $C_{27}H_{30}ClFN_5O_3Ru$ requires 628.1).

Complex 8. Yellow powder (100.2 mg, 47.9%). Anal. Calc. for $C_{28}H_{31}Cl_2F_7N_5O_2Pru\ H_2O$: C, 40.84; H, 4.04; N, 8.50%. Found: C, 40.78; H, 4.11; N, 8.47. ^{1}H NMR (d_6-DMSO, 400 MHz) δ (ppm): 8.69 (s, 1 H), 8.08 (dd, J_1 = 6.8 Hz, J_2 = 4.8 Hz, 1 H), 7.98 (s, 1 H), 7.77–7.73 (m, 1 H), 7.52 (t, J = 9.2 Hz, 1 H), 7.31 (s, 1 H), 7.07 (br s, 1 H), 6.49 (br s, 1 H), 5.80 (d, J = 5.2 Hz, 1 H), 5.77 (d, J = 6.0 Hz, 1 H), 5.68 (t, J = 5.2 Hz, 1 H), 5.64 (t, J = 5.2 Hz, 1 H), 4.42 (s, 2 H), 4.04 (s, 1 H), 3.96 (s, 1 H), 3.86 (s, 1 H), 3.53–3.48 (m, 2 H), 3.30–3.20 (m, 2 H), 2.81–2.75 (m, 2 H), 2.33–2.27 (m, 1 H), 2.09–2.06 (m, 1 H), 2.00–1.97 (m, 1 H). ^{13}C NMR (d_6-DMSO, 100 MHz) δ (ppm): 157.4, 155.8, 152.0, 148.7, 136.1, 125.3, 124.1, 119.6, 117.3, 108.5, 104.0, 103.2, 101.0, 100.9, 83.3, 82.3, 81.3, 79.8, 79.2, 78.5, 68.1, 56.8, 56.0, 53.7, 52.1, 45.5, 29.7, 22.7. MS (MALDI-TOF) (m/z): 660.2 (M^+, $C_{28}H_{31}Cl_2FN_5O_2Ru$ requires 660.1); 624.2 ($[M - HCl]^+$, $C_{28}H_{30}ClFN_5O_2Ru$ requires 624.1).

Complex 9. Yellow powder (47.9 mg, 22.4%). Anal. Calc. for $C_{28}H_{33}Cl_2F_7N_5O_3PRu{\cdot}3H_2O$: C, 38.32; H, 4.48; N, 7.98%. Found: C, 38.26; H, 4.53; N, 8.05. ^{1}H NMR (d_6-DMSO, 400 MHz) δ (ppm): 8.84 (s, 1 H), 8.03 (s, 1 H), 8.01 (dd, J_1 = 6.8 Hz, J_2 = 2.4 Hz, 1 H), 7.71–7.68 (m, 1 H), 7.57 (t, J = 9.2 Hz, 1 H), 7.27 (d, J = 5.2 Hz, 1 H), 7.05 (br s, 1 H), 6.64 (br s, 1 H), 5.87–5.82 (m, 2 H), 5.60–5.57 (m, 2 H), 5.55–5.53 (m, 1 H), 4.68 (br s, 1 H), 4.41–4.25 (m, 3 H), 4.03 (s, 3 H), 3.98 (s, 2 H), 3.70–3.65 (m, 3 H), 3.38–3.24 (m, 2 H), 3.08–2.99 (m, 1 H), 2.80–2.65 (m, 1 H), 2.60–2.54 (m, 2 H), 2.27–2.16 (m, 2 H). ^{13}C NMR (d_6-DMSO, 100 MHz) δ (ppm): 158.4, 156.8, 156.7, 150.3, 149.7, 126.7, 125.4, 119.7, 117.7, 117.5, 107.8, 104.2, 101.4, 100.2, 85.8, 84.6, 84.0, 83.5, 81.7, 79.5, 67.7, 60.5, 57.1, 52.4, 50.4, 45.7, 36.4, 28.1. MS (MALDI-TOF) (m/z): 678.2 (M^+, $C_{28}H_{33}Cl_2FN_5O_3Ru$ requires 678.1); 642.2 ($[M - HCl]^+$, $C_{28}H_{32}Cl_2FN_5O_3Ru$ requires 642.1).

Complex 10. Yellow powder (71.6 mg, 33.2%). Anal. Calc. for $C_{29}H_{33}Cl_2F_7N_5O_2PRu{\cdot}2H_2O$: C, 40.71; H, 4.36; N, 8.19%. Found: C, 40.63; H, 4.47; N, 8.26. ^{1}H NMR (d_6-DMSO, 400 MHz) δ (ppm): 9.58 (s, 1 H), 8.52 (s, 1 H), 8.13 (dd, J_1 = 6.8 Hz, J_2 = 2.4 Hz, 1 H), 7.87 (s, 1 H), 7.83–7.80 (m, 1 H), 7.47 (t, J = 9.2 Hz, 1 H), 7.25 (s, 1 H), 6.57 (br s, 1 H), 5.83–5.80 (m, 1 H), 5.80–5.77 (m, 2 H), 5.72–5.70 (m, 1 H), 4.35 (br s, 1 H), 4.25 (br s, 1 H), 3.98 (s, 1 H), 3.93 (s, 3 H), 3.71 (s, 1 H), 2.84–2.55 (m, 6 H), 2.07–1.96 (m, 2 H). ^{13}C NMR (d_6-DMSO, 100 MHz) δ (ppm): 156.6, 154.9, 153.1, 148.5, 137.2, 124.0, 122.7, 119.4, 117.2, 109.2, 107.7, 103.0, 101.4, 99.6, 84.8, 82.5, 81.8, 79.9, 79.5, 79.2, 67.6, 56.4, 56.4, 55.9, 55.5, 29.8, 29.6, 28.1, 22.7. MS (MALDI-TOF) (m/z): 674.2 (M^+, $C_{29}H_{33}Cl_2FN_5O_2Ru$ requires 674.1); 638.2 ($[M - HCl]^+$, $C_{29}H_{32}ClFN_5O_2Ru$ requires 638.1).

Complex 11. Yellow powder (115.1 mg, 60.1%). Anal. Calc. for $C_{26}H_{28}ClF_6N_6O_2PRu{\cdot}4H_2O$: C, 38.55; H, 4.48; N, 10.37%. Found: C, 38.47; H, 4.54; N, 10.21. ^{1}H NMR (d_6-DMSO, 400 MHz) δ (ppm): 8.84 (s, 1 H), 8.29 (s, 1 H), 8.10 (s, 1 H), 8.05 (d, J = 8.0 Hz, 1 H), 7.73 (d, J = 4.0 Hz, 1 H), 7.71 (s, 1 H), 7.42 (br s, 1 H), 5.79 (s, 6 H), 4.49 (m, 2 H), 4.06 (s, 3 H), 3.86 (s, 1 H), 3.63–3.53 (m, 2 H), 3.27 (s, 1 H), 2.71 (s, 2 H), 2.39–2.29 (m, 1 H), 2.10–1.97 (m, 1 H). ^{13}C NMR (d_6-DMSO, 100 MHz) δ (ppm): 158.3, 156.8, 149.2, 130.8, 129.7, 129.2, 126.9, 118.9, 112.1, 111.7, 108.1, 104.8, 104.6, 104.1, 100.0, 83.9 (6 C), 68.4, 57.1, 53.5, 51.9, 46.0. MS (MALDI-TOF) (m/z): 593.1 (M^+, $C_{26}H_{28}ClN_6O_2Ru$ requires 593.1); 557.2 ($[M - HCl]^+$, $C_{26}H_{27}N_6O_2Ru$ requires 557.1).

Complex 12. Yellow powder (46.0 mg, 22.3%). Anal. Calc. for $C_{30}H_{36}ClF_6N_6O_2PRu{\cdot}H_2O$: C, 44.37; H, 4.72; N, 10.35%. Found: C, 44.48; H, 4.67; N, 10.28. ^{1}H NMR (d_6-DMSO, 400 MHz) δ (ppm): 8.70 (s, 1 H), 8.33 (s, 1 H), 8.10–8.09 (m, 1 H), 7.99 (s, 1 H), 7.69–7.65 (m, 2 H), 7.33 (s, 1 H), 6.56 (br s, 1 H), 5.68 (d, J = 6.0 Hz, 1 H), 5.64 (d, J = 6.0 Hz, 1 H), 5.61 (d, J = 6.0 Hz, 1 H), 5.56 (d, J = 6.0 Hz, 1 H), 4.47 (br s, 1 H), 4.39 (br s, 1 H), 4.04 (s, 3 H), 4.00–3.96 (m, 1 H), 3.88–3.83 (m, 1 H), 3.69–3.57 (m, 1 H), 2.87–2.82 (m, 1 H), 2.73–2.71 (m, 1 H), 2.23 (s, 3 H), 2.21 (s, 1 H), 2.15 (d, J = 4.0 Hz, 1 H), 2.09 (m, 1 H), 1.22 (d, J = 2.4 Hz, 3 H), 1.21 (d, J = 2.4 Hz, 3 H). ^{13}C NMR (d_6-DMSO, 100 MHz) δ (ppm): 157.3, 155.7, 152.1, 148.7, 140.0, 130.6, 128.2, 127.8, 126.2, 119.1, 112.0, 108.8, 104.6, 103.8, 96.7, 83.6, 82.3, 81.9, 81.5, 81.2, 80.7, 67.6, 56.8, 54.6, 51.4, 45.8, 30.5, 22.8, 22.2, 17.4. MS (MALDI-TOF) (m/z): 649.2 (M^+, $C_{30}H_{36}ClN_6O_2Ru$ requires 649.2); 613.2 ($[M - HCl]^+$, $C_{30}H_{35}N_6O_2Ru$ requires 613.2).

Complex 13. Yellow powder (52.2 mg, 24.7%). Anal. Calc. for $C_{26}H_{31}ClF_6N_5O_3PRu{\cdot}2H_2O$: C, 40.08; H, 4.53; N, 8.99%. Found: C, 39.87; H, 4.60; N, 9.18. ^{1}H NMR (d_6-DMSO, 400 MHz) δ (ppm): 8.81 (s, 1 H), 8.12 (s, 1 H), 7.44–7.39 (m, 2 H), 7.32–7.25 (m, 2 H), 6.91 (d, J = 8.4 Hz, 1 H), 6.86 (br s, 1 H), 5.79 (s, 6 H), 4.54–4.37 (m, 2 H), 4.06 (s, 3 H), 3.98–3.88 (m, 2 H), 3.81 (s, 3 H), 3.60–3.48 (m, 3 H), 2.76–2.64 (m, 2 H), 2.40–2.27 (m, 1 H), 2.09–1.96 (m, 1 H). ^{13}C NMR (d_6-DMSO, 100 MHz) δ (ppm): 160.0, 158.5, 156.7, 150.2, 149.2, 138.5, 137.6, 130.2, 117.2, 112.1, 111.1, 107.8, 104.8, 101.6. 83.9 (6 C), 68.4, 57.1, 55.8, 53.5, 51.8, 46.0. MS (MALDI-TOF) (m/z): 598.1 (M^+, $C_{26}H_{31}ClN_5O_3Ru$ requires 598.1); 562.2 ($[M - HCl]^+$, $C_{26}H_{30}N_5O_3Ru$ requires 562.1).

Complex 14. Yellow powder (49.9 mg, 24.1%). Anal. Calc. for $C_{29}H_{35}ClF_6N_5O_3PRu{\cdot}2H_2O$: C, 42.99; H, 4.73; N, 8.64%. Found: C, 42.72; H, 5.08; N, 8.28. ^{1}H NMR (d_6-DMSO, 400 MHz) δ (ppm): 9.45 (s, 1 H), 8.50 (s, 1 H), 7.95 (s, 1 H), 7.49 (s, 1 H), 7.32–7.29 (m, 4 H), 6.48 (br s, 1 H), 5.81–5.77 (m, 2 H), 5.70–5.68 (m, 1 H), 5.64–5.55 (m, 1 H), 4.45–4.40 (m, 2 H), 4.00 (s, 3 H), 3.92–3.84 (m, 4 H), 3.79 (s, 3 H), 2.78–2.66 (m, 4 H). ^{13}C NMR (d_6-DMSO, 100 MHz) δ (ppm): 159.9, 156.9, 154.8, 153.6, 148.0, 147.8, 141.0, 129.7, 126.4, 124.7, 115.0, 108.7, 103.2, 101.1, 85.3, 84.2, 82.2, 81.3, 79.9, 79.1, 67.9, 56.5, 55.7, 55.6, 53.9, 52.0, 45.6, 29.7, 22.7. MS (MALDI-TOF) (m/z): 638.2 (M^+, $C_{29}H_{35}ClN_5O_3Ru$ requires 638.2); 602.2 ($[M - HCl]^+$, $C_{29}H_{34}N_5O_3Ru$ requires 602.2).

Hydrolysis studies

The kinetic studies on the hydrolysis of complexes **7–14** was carried out using a UV-2550 spectrometer (Shimadzu, Japan). Firstly, each complex being tested was dissolved in DMSO with a concentration of 5 mM, an aliquot (10 μL) of the DMSO solution was then added to 990 μL deionized water in a quartz cuvette and the UV-Vis spectrum of the mixture was immediately recorded by scanning over the wavelength region from 200–500 nm at 5 minute intervals. The wavelength corresponding to the maximum change in absorbance of each hydrolysis reaction was selected for the measurement of the rate constant. The samples used for the rate constant measurements were prepared by the same procedure as described above, and the absorbance at selected wavelengths was then recorded at 5 minute intervals. The absorbance/time data for each hydrolysis reaction were computer-fitted to the first-order rate equation, giving the k_{H_2O} value (k) for the hydrolysis reaction.

Enzyme-linked immunosorbent assay (ELISA)

The EGFR solution in 50% glycerol, containing 50 mM HEPES (pH = 7.6), 150 mM NaCl, 0.1% Triton and 1 mM dithiothreitol (DTT) was purchased from Sigma Chemical Company; Signal Transduction Protein (Tyr66) biotinylated peptide, Phospho-Tyrosine Mouse mAb (P-Tyr-100), HTScan® Tyrosine Kinase Buffer (4×), Adenosine-triphosphate (ATP), and DL-Dithiothreitol (DTT) from Cell Signalling Company; HRP-labelled Goat Anti-Mouse lgG (H + L) from Zhongshan Golden Bridge Biotechnology Co. Ltd (China); Bovine Serum Albumin (BSA), and 3,3′,5,5′-tetramethylbenzidine (TMB) from Xinjingke Biotechnology Co. Ltd (China), and Streptavidin from Tianjin Biotechnology Co. Ltd (China); 96-well plates were purchased from Beijing BioDee BioTech Co. Ltd.

The ELISA screening was performed following the instructions provided by the supplier of the assay kits (no. 7909, Cell Signalling Technology, Inc.). An aliquot (10 μL) of the enzyme solution was added to 415 μL DTT kinase buffer which consisted of 1.25 M DTT and 4 × HTScan® Tyrosine Kinase Buffer (240 mM HEPES (pH 7.5), 20 mM $MgCl_2$, 20 mM $MnCl_2$, and 12 μM Na_3VO4). Each tested complex was dissolved in dimethylsulfoxide (DMSO) to give a 4 mM solution which was then diluted by deionized water prior to use. The ATP/peptide mixture was prepared by the addition of 10 μL of 10 mM ATP to 125 μL of 6 μM substrate peptide, and then diluted with D_2O to 250 μL. An aliquot (12.5 μL) of the solution of a tested compound was mixed with the as-prepared EGFR solution (12.5 μL) and incubated at 298 K for 5 minutes, followed by the addition of 25 μL of the ATP/substrate mixture, and then the resulting mixture was incubated at 310 K for 1 h. The phosphorylation reaction was terminated by the addition of 50 μL per well of buffer (50 mM EDTA, pH = 8). Each well of a microtitre plate was coated with 100 μL of 10 μg mL^{-1} streptavidin in carbonate–bicarbonate buffer and incubated overnight at 277 K, and then blocked with 1.5% bovine serum albumin (BSA) in PBS/T (PBS solution containing 0.05% Tween-20) at 310 K for 2 h, followed by washing three times with PBS/T prior to use. Then, 25 μL per well of each enzymatic reaction mixture and 75 μL per well of D_2O were added to the plate (in triplicate) for incubation at 310 K for 1 h. Following washing three times with PBS/T, 100 μL of the primary antibody (Phospho-Tyrosine Mouse mAb, 1 : 1000 in PBS/T with 1.5% BSA) was added to each well and the plate was incubated at 310 K for another 1 h. The plate was again washed three times with PBS/T, and then 100 μL of the secondary antibody (HRP-labelled Goat Anti-Mouse lgG, 1 : 1000 in PBS/T with 1.5% BSA) was added to each well for 1 h of incubation at 310 K, followed by washing three times with PBS/T. Finally, 100 μL of the TMB substrate was added to each well and the plate was incubated at 310 K for 15 min, and then the reaction was stopped by the addition of 100 μL of 2 M H_2SO_4 to each well, and the plate was read on the ELISA plate reader (SpectraMax M5 Molecular Devices Corporation) at 450 nm to determine the OD values.

In vitro anti-proliferation assay

The human breast cancer cell line HeLa was obtained from the Centre for Cell Resource of Peking Union Medical College Hospital. HeLa cells were maintained in a DMEM (Invitrogen, USA) medium supplemented with 10% fetal calf serum (HyClone, USA). If requested, an aliquot of 100 ng mL^{-1} epidermal growth factor (Sigma, USA) was added into the media. The cells were grown at 310 K in a humidified atmosphere containing 5% CO_2 for 2 days prior to the screening experiments.

The IC_{50} values, which are the concentrations of the tested compounds that inhibit 50% of cell growth, were determined using a 3-(4,5-dimethyl-2-thiazolyl)-2,5-diphenyl-2-*H*-tetrazolium bromide (MTT) assay. Cells were plated at a density of 4000 cells per well in a 100 μL medium in 96-well plates and grew in the absence or in the presence of 100 ng mL^{-1} EGF for 24 h. The stock solutions [20 mM, except for cisplatin (1 mM)] of all the tested compounds were made up fresh in DMSO before being diluted down in the medium to give the required concentration for addition to the cells and the final concentration of DMSO in the medium was 1%. Then cells were exposed to each tested compound at eight concentrations for 48 h. The resulting solution was removed and washed three times using PBS, then the 100 μL cell culture medium containing MTT (0.5 mg ml^{-1}) was added to each well and incubated at 310 K for 4 h. After that, the MTT medium was removed and 100 μL DMSO was added to each well to dissolve the formazan

crystals at ambient temperature for 10 min. Optical density (OD) values were measured using a microplate reader (SpectraMax M5 Molecular Devices Corporation) at a wavelength of 570 nm. The inhibition rate (IR) was calculated based on the equation as follows: IR (%) = $[1 - (OD_{compound} - OD_{blank})/(OD_{control} - OD_{blank})] \times 100\%$.

All reported values were averages of three independent experiments and expressed as mean ± SD (standard deviation).

The *in vitro* antiproliferative activity of complexes **7–14** on the human bronchial epithelial (HBE) cell line (gifted by Dr Li Xu at ICCAS) was characterised using the same MTT method described above.

High performance liquid chromatography (HPLC)

An Agilent 1200 series quaternary pump, a Rheodyne sample injector with a 20 μL loop, an Agilent 1200 series UV-Vis DAD detector and a Chemstation data processing system were used. The mobile phases were water containing 0.1% TFA (solvent A) and acetonitrile containing 0.1% TFA (solvent B). The separation of the hydrolytic adducts of complexes **7–14** was carried out on an Agilent Eclipse XDB-C18 reversed-phase column (4.6 × 150 mm, 5 μm, Agilent Technologies). The gradient (B) was: 10% to 80% from 0 to 20 min, keeping at 80% up to 22 min, and finally resetting to 10% at 25 min.

Circular dichroism spectroscopy

Complexes **4** and **8** were dissolved in DMSO to yield a 20 mM stock solution, then diluted using a 5 mM Tris-HCl (pH 7.4) buffer to the appropriate concentrations. Calf thymus DNA (ctDNA) was dissolved directly in the 5 mM Tris-HCl (pH 7.4) buffer. The DNA concentration (in base pairs) was determined by UV-Vis spectroscopy. The CD spectra data were obtained using a J-815 CD spectrometer (JASCO). The ctDNA solutions (200 μM) were incubated with different concentrations of complex **4** or **8** in Tris buffer at 310 K for 24 h, and then CD spectra of ctDNA were acquired in the wavelength region of 200–400 nm with the following parameters: bandwidth, 2 nm; step-size, 0.5 nm; time-per-point, 0.5 s.[45]

Fluorescent titration assay

Fluorescence spectroscopy was performed using a HITACHI F-4500 fluorescence spectrophotometer (Japan). Operation parameters: EX Slit, 5.0 nm; EM Slit, 5.0 nm; PMT Voltage, 700 V. In the competition studies, a solution containing 20 μM of Hoechst33342 and 200 μM of ctDNA was titrated with varying concentrations of complex **4** or **8** from 0 to 120 μM in a Tris-HCl (5 mM, pH 7.4) buffer. The ctDNA–Hoechst complex was excited at 370 nm and the emission spectra were recorded from 400 to 650 nm. The Stern–Volmer constant (K_{sv}) was used to evaluate the fluorescence quenching efficiency. The classical Stern–Volmer equation:

$$F_0/F = 1 + K_{SV}\,[Q]$$

where F_0 and F are the fluorescence intensities before and after the addition of the quencher, respectively. $[Q]$ is the concentration of the quencher, and K_{sv} is the quenching constant.

Elemental analysis and NMR spectroscopy

Elemental analysis was performed using a Flash EA 1112 element analysis instrument (ThermoQuest). NMR spectra were obtained with a Bruker Avance III HD 400 spectrometer (Germany).

Molecular modelling

The docking analysis was performed using the Surflex-Dock module, a fully automatic docking tool available on the Sybyl-X 1.1 programme (Tripos Inc.), running on a Dual-core Intel(R) E5300 CPU (2.60 GHz) and RAM Memory (2 GB) under the Windows XP system. The crystal structures of the EGFR-erlotinib complex and B-form dodecamer duplex, $d(CGCGAATTCGCG)_2$ (**I**), were retrieved from PDB under the codes 1M17 [53] and 1BNA,[51] respectively. All the hydrogen atoms were added to define the correct configuration and tautomeric states. After adding the charge, the modelled structure was energy-minimized using the Powell energy minimization algorithm with an AMBER7 FF99 force field for the EGFR-erlotinib complex and a Tripos force field for DNA, respectively.

For the docking to EGFR analysis, the binding ligand erlotinib was extracted and the docking pocket was generated at the ATP binding cleft automatically. Then complexes **1–14** and their hydrolytic adducts built by the Sybyl programme were individually docked into the pocket for docking analysis.

The binding pocket at the minor groove of duplex **I** was generated automatically after removing the water, covering the base-pairs G2–C23 (top) to C9–G16 (bottom).[51] Then complexes **1–14** and their hydrolytic adducts were individually docked into the pocket for docking analysis. The binding energy to G4–N7 in the DNA duplex was calculated based on the equation as follows: $\Delta E = E_3 - (E_2 + E_1)$, where E_3 is the energy of the DNA–ligand complex; E_2 the energy of the DNA receptor; and E_1 the energy of the ligand. Molecular energy (E) was calculated using the Powell energy minimization algorithm with a Tripos force field, a distance dependent dielectric function and Gasteiger-Huckel charges. All the energy values were returned in the form of kcal mol^{-1}.

Acknowledgements

We thank NSFC (Grant no. 21135006, 21127901, 21275148, 21301181 and 21321003), the 973 Program of MOST (2013CB531805) for support, and Professor Peter Sadler and Dr Abraha Habtemariam at the University of Warwick for the gifted arene ruthenium dimers and stimulated discussion.

Notes and references

1 R. E. Aird, J. Cummings, A. A. Ritchie, M. Muir, R. E. Morris, H. Chen, P. J. Sadler and D. I. Jodrell, *Br. J. Cancer*, 2002, **86**, 1652–1657.
2 E. Alessio, G. Mestroni, A. Bergamo and G. Sava, *Curr. Top. Med. Chem.*, 2004, **4**, 1525–1535.

3 P. C. A. Bruijnincx and P. J. Sadler, *Curr. Opin. Chem. Biol.*, 2008, **12**, 197–206.
4 F. Caruso, M. Rossi, A. Benson, C. Opazo, D. Freedman, E. Monti, M. B. Gariboldi, J. Shaulky, F. Marchetti, R. Pettinari and C. Pettinari, *J. Med. Chem.*, 2012, **55**, 1072–1081.
5 P. J. Dyson and G. Sava, *Dalton Trans.*, 2006, 1929–1933.
6 G. Gasser, I. Ott and N. Metzler-Nolte, *J. Med. Chem.*, 2010, **54**, 3–25.
7 C. G. Hartinger and P. J. Dyson, *Chem. Soc. Rev.*, 2009, **38**, 391–401.
8 C. G. Hartinger, N. Metzler-Nolte and P. J. Dyson, *Organometallics*, 2012, **31**, 5677–5685.
9 G. Sava, A. Bergamo and P. J. Dyson, *Dalton Trans.*, 2011, **40**, 9069–9075.
10 G. S. Smith and B. Therrien, *Dalton Trans.*, 2011, **40**, 10793–10800.
11 F. Y. Wang, A. Habtemariam, E. P. L. van der Geer, R. Fernandez, M. Melchart, R. J. Deeth, R. Aird, S. Guichard, F. P. A. Fabbiani, P. Lozano-Casal, I. D. H. Oswald, D. I. Jodrell, S. Parsons and P. J. Sadler, *Proc. Natl. Acad. Sci. U. S. A.*, 2005, **102**, 18269–18274.
12 C. G. Hartinger, S. Zorbas-Seifried, M. A. Jakupec, B. Kynast, H. Zorbas and B. K. Keppler, *J. Inorg. Biochem.*, 2006, **100**, 891–904.
13 M. A. Jakupec, M. Galanski, V. B. Arion, C. G. Hartinger and B. K. Keppler, *Dalton Trans.*, 2008, 183–194.
14 G. Sava, A. Bergamo, S. Zorzet, B. Gava, C. Casarsa, M. Cocchietto, A. Furlani, V. Scarcia, B. Serli, E. Iengo, E. Alessio and G. Mestroni, *Eur. J. Cancer*, 2002, **38**, 427–435.
15 C. G. Hartinger, M. A. Jakupec, S. Zorbas-Seifried, M. Groessl, A. Egger, W. Berger, H. Zorbas, P. J. Dyson and B. K. Keppler, *Chem. Biodiversity*, 2008, **5**, 2140–2155.
16 E. S. Antonarakis and A. Emadi, *Cancer Chemother. Pharmacol.*, 2010, **66**, 1–9.
17 H. M. Chen, J. A. Parkinson, S. Parsons, R. A. Coxall, R. O. Gould and P. J. Sadler, *J. Am. Chem. Soc.*, 2002, **124**, 3064–3082.
18 A. Habtemariam, M. Melchart, R. Fernandez, S. Parsons, I. D. H. Oswald, A. Parkin, F. P. A. Fabbiani, J. E. Davidson, A. Dawson, R. E. Aird, D. I. Jodrell and P. J. Sadler, *J. Med. Chem.*, 2006, **49**, 6858–6868.
19 R. E. Morris, R. E. Aird, P. D. Murdoch, H. M. Chen, J. Cummings, N. D. Hughes, S. Parsons, A. Parkin, G. Boyd, D. I. Jodrell and P. J. Sadler, *J. Med. Chem.*, 2001, **44**, 3616–3621.
20 W. H. Ang, L. J. Parker, A. De Luca, L. Juillerat-Jeanneret, C. J. Morton, M. Lo Bello, M. W. Parker and P. J. Dyson, *Angew. Chem., Int. Ed.*, 2009, **48**, 3854–3857.
21 B. Biersack, M. Zoldakova, K. Effenberger and R. Schobert, *Eur. J. Med. Chem.*, 2010, **45**, 1972–1975.
22 H. Bregman, D. S. Williams, G. E. Atilla, P. J. Carroll and E. Meggers, *J. Am. Chem. Soc.*, 2004, **126**, 13594–13595.
23 T. Bugarcic, A. Habtemariam, J. Stepankova, P. Heringova, J. Kasparkova, R. J. Deeth, R. D. L. Johnstone, A. Prescimone, A. Parkin, S. Parsons, V. Brabec and P. J. Sadler, *Inorg. Chem.*, 2008, **47**, 11470–11486.
24 A. Kurzwernhart, W. Kandioller, C. Bartel, S. Bachler, R. Trondl, G. Muhlgassner, M. A. Jakupec, V. B. Arion, D. Marko, B. K. Keppler and C. G. Hartinger, *Chem. Commun.*, 2012, **48**, 4839–4841.
25 E. Meggers, *Curr. Opin. Chem. Biol.*, 2007, **11**, 287–292.
26 A. F. A. Peacock, A. Habtemariam, R. Fernandez, V. Walland, F. P. A. Fabbiani, S. Parsons, R. E. Aird, D. I. Jodrell and P. J. Sadler, *J. Am. Chem. Soc.*, 2006, **128**, 1739–1748.
27 Y. K. Yan, M. Melchart, A. Habtemariam and P. J. Sadler, *Chem. Commun.*, 2005, 4764–4776.
28 F. Y. Wang, H. M. Chen, J. A. Parkinson, P. D. Murdoch and P. J. Sadler, *Inorg. Chem.*, 2002, **41**, 4509–4523.
29 W. H. Ang and P. J. Dyson, *Eur. J. Inorg. Chem.*, 2006, 4003–4018.
30 K. J. Kilpin, S. M. Cammack, C. M. Clavel and P. J. Dyson, *Dalton Trans.*, 2013, **42**, 2008–2014.
31 C. Scolaro, A. Bergamo, L. Brescacin, R. Delfino, M. Cocchietto, G. Laurenczy, T. J. Geldbach, G. Sava and P. J. Dyson, *J. Med. Chem.*, 2005, **48**, 4161–4171.
32 S. Lu, W. Zheng, L. Ji, Q. Luo, X. Hao, X. Li and F. Wang, *Eur. J. Med. Chem.*, 2013, **61**, 84–94.
33 W. Zheng, Q. Luo, Y. Lin, Y. Zhao, X. L. Wang, Z. F. Du, X. Hao, Y. Yu, S. Lu, L. Y. Ji, X. C. Li, L. Yang and F. Y. Wang, *Chem. Commun.*, 2013, **49**, 10224–10226.
34 A. E. Wakeling, S. P. Guy, J. R. Woodburn, S. E. Ashton, B. J. Curry, A. J. Barker and K. H. Gibson, *Cancer Res.*, 2002, **62**, 5749–5754.
35 M. Muhsin, J. Graham and P. Kirkpatrick, *Nat. Rev. Drug Discovery*, 2003, **2**, 515–516.
36 V. Chandregowda, A. K. Kush and G. Chandrasekara Reddy, *Eur. J. Med. Chem.*, 2009, **44**, 3046–3055.
37 H. M. Chen, J. A. Parkinson, O. Novakova, J. Bella, F. Y. Wang, A. Dawson, R. Gould, S. Parsons, V. Brabec and P. J. Sadler, *Proc. Natl. Acad. Sci. U. S. A.*, 2003, **100**, 14623–14628.
38 H. K. Liu, S. J. Berners-Price, F. Y. Wang, J. A. Parkinson, J. J. Xu, J. Bella and P. J. Sadler, *Angew. Chem., Int. Ed.*, 2006, **45**, 8153–8156.
39 F. Y. Wang, J. J. Xu, A. Habtemariam, J. Bella and P. J. Sadler, *J. Am. Chem. Soc.*, 2005, **127**, 17734–17743.
40 F. Wang, H. M. Chen, S. Parsons, L. D. H. Oswald, J. E. Davidson and P. J. Sadler, *Chem. – Eur. J.*, 2003, **9**, 5810–5820.
41 H. K. Liu, J. A. Parkinson, J. Bella, F. Y. Wang and P. J. Sadler, *Chem. Sci.*, 2010, **1**, 258–270.
42 H. K. Liu and P. J. Sadler, *Acc. Chem. Res.*, 2011, **44**, 349–359.
43 J. Kypr, I. Kejnovska, D. Renciuk and M. Vorlickova, *Nucleic Acids Res.*, 2009, **37**, 1713–1725.
44 O. Novakova, H. M. Chen, O. Vrana, A. Rodger, P. J. Sadler and V. Brabec, *Biochemistry*, 2003, **42**, 11544–11554.
45 B. Selvakumar, V. Rajendiran, P. U. Maheswari, H. Stoeckli-Evans and M. Palaniandavar, *J. Inorg. Biochem.*, 2006, **100**, 316–330.
46 T. Sarwar, M. A. Husain, S. U. Rehman, H. M. Ishqi and M. Tabish, *Mol. BioSyst.*, 2015, **11**, 522–531.

47 A. H. Kesarwala, M. M. Samrakandi and D. Piwnica-Worms, *Cancer Res.*, 2009, **69**, 976–983.
48 A. N. Jain, *J. Comput. Aided Mol. Des.*, 2009, **23**, 355–374.
49 M. A. Miteva, W. H. Lee, M. O. Montes and B. O. Villoutreix, *J. Med. Chem.*, 2005, **48**, 6012–6022.
50 A. N. Jain, *J. Comput. Aided Mol. Des.*, 1996, **10**, 427–440.
51 H. R. Drew, R. M. Wing, T. Takano, C. Broka, S. Tanaka, K. Itakura and R. E. Dickerson, *Proc. Natl. Acad. Sci. U. S. A.*, 1981, **78**, 2179–2183.
52 K. Wu, Q. Luo, W. B. Hu, X. C. Li, F. Y. Wang, S. X. Xiong and P. J. Sadler, *Metallomics*, 2012, **4**, 139–148.
53 J. Stamos, M. X. Sliwkowski and C. Eigenbrot, *J. Biol. Chem.*, 2002, **277**, 46265–46272.
54 S. Mallena, M. P. H. Lee, C. Bailly, S. Neidle, A. Kumar, D. W. Boykin and W. D. Wilson, *J. Am. Chem. Soc.*, 2004, **126**, 13659–13669.
55 C. Gossens, I. Tavernelli and U. Rothlisberger, *J. Am. Chem. Soc.*, 2008, **130**, 10921–10928.